Optics Letters

Signal-to-noise ratio enhancement of stimulated Brillouin scattering based pulse compression of an ultrabroad microwave signal by use of a dispersion compensation fiber

YI JI, WEIWEN ZOU,* XIN LONG, AND JIANPING CHEN

State Key Laboratory of Advanced Optical Communication Systems and Networks, Department of Electronic Engineering, Shanghai Jiao Tong University, Shanghai 200240, China
**Corresponding author: wzou@sjtu.edu.cn*

Received 22 May 2017; revised 26 June 2017; accepted 2 July 2017; posted 3 July 2017 (Doc. ID 296183); published 26 July 2017

The signal-to-noise ratio (SNR) of all-optical pulse compression of broadband microwave signals based on stimulated Brillouin scattering (SBS) is theoretically analyzed. According to numerical simulation, it is found that the SNR is dominantly determined by the Brillouin gain coefficient g_B. With the improvement of g_B, the SNR is evidently enhanced and the bandwidth of SBS-based pulse compression is consequently enlarged. Experiments are implemented by using a dispersion compensation fiber with a higher g_B rather than a single-mode fiber. The experimental results show that better SNR of the compressed signal is obtained and the system bandwidth is extended up to 5 GHz.

OCIS codes: (070.1170) Analog optical signal processing; (190.0190) Nonlinear optics; (290.5900) Scattering, stimulated Brillouin.

https://doi.org/10.1364/OL.42.002980

As an important signal processing method, pulse compression technology has been widely used in the radar field [1,2]. So far, digital processing and surface processing are mature methods to fulfill the pulse compression of complicated signals [3–5]. However, modern coherent radar systems are faced with significant issues of signal processing, such as increased bandwidth, the challenge of digital storage, and fast signal processing [2,6,7]. Although the developed photonic analog-to-digital conversion (ADC) has overcome the bandwidth limitation of the electronic ADC [8–10], the challenge of digital storage and fast signal processing remains unchanged. Therefore, an advanced pulse compression technique is needed. Thanks to the development of microwave photonics [11], broadband microwave signals with high phase stability can be generated, controlled, and processed [12–17]. For instance, a novel pulse compression process for broadband microwave signals based on stimulated Brillouin scattering (SBS) was theoretically and experimentally demonstrated in [16]. SBS is, in principle, three-wave interaction among the pump lightwave, the counter-propagated probe lightwave, and the acoustic wave [18]. The acoustic wave inherits the amplitude and phase information of the lightwaves. Subsequently, during the re-coupling between this acoustic wave and pump lightwave, the time delay and amplitude conjugation conditions, which are necessary for the matched filtering, are automatically satisfied. Thus, the pump lightwave carrying the microwave signal amplifies the short-pulse probe lightwave via the acoustic wave. Consequently, the pulse compression is implemented by direct detection of the probe pulse with and without SBS. The advantages of this pulse compression technique in [16] are the short processing time and, thus, significant reduction of the difficulty of digital storage and signal processing. A proof-of-concept experiment was carried out to validate the pulse compression of an LFM pulse. However, the compressed signal is severely distorted especially by noise effect; thus, the system bandwidth is limited to 1 GHz.

Compared to [16], the theory of the SBS-based pulse compression technique is improved by implementing the numerical analysis of the detected probe signal considering the noise contribution and deriving the signal-to-noise ratio (SNR) of the compressed signal. The higher Brillouin gain coefficient g_B contributes to a higher SNR and, thus, a broader system bandwidth. Experimentally, a dispersion compensation fiber (DCF) with a higher g_B [19] rather than the single-mode fiber (SMF) utilized in [16] is used to verify the enhanced theory. The experimental result shows that the SNR of the compressed signal can be enhanced due to the higher g_B. Consequently, the system bandwidth can be significantly extended up to 5 GHz.

In [16], the basic theory of SBS-based all-optical pulse compression was demonstrated. However, the noise effect was not considered. Suppose that $n_1(t)$ and $n_2(t)$ denote the noise of the injected pump and probe lightwaves, respectively. The complex envelope of the injected pump $E_{nP0}(t)$ and probe $E_{nS0}(t)$ lightwaves can be expressed by

$$\begin{cases} E_{nP0}(t) = E_{P0}(t) + n_1(t) \\ E_{nS0}(t) = E_{S0}(t) + n_2(t) \end{cases}, \tag{1}$$

where $E_{P0}(t)$ and $E_{S0}(t)$ are the ideal envelopes of the pump and probe lightwaves, respectively, without considering the noise effect.

After substituting Eq. (1) into the three-wave coupling equations describing the SBS interaction in the fiber, namely, Eqs. (1)–(3) in [16], the electric field of the detected probe lightwaves $E'_{nS}(t+T)$ suffering the SBS gain can be written as

$$E'_{nS}(t+T) = \frac{g_B v}{8\tau_p}\{E_{S0}(t) \otimes [u(t)y_P(t)e^{-\Gamma^* t}] + N_1(t)\} + E_{nS0}(t), \tag{2}$$

where v denotes the light velocity in the fiber, τ_p represents the phonon lifetime, Γ represents the detuning and dumping coefficient, and $y_P(t) = E_{P0}(t) \otimes E^*_{P0}(-t)$ is the ideal pulse compression of the signal to be processed. Moreover, $N_1(t)$ corresponds to the noise generated through the compression process, which is given by the following:

$$\begin{aligned} N_1(t) = {} & E_{S0}(t) \otimes \{u(t)[E_{P0}(t) \otimes n_1^*(-t) \\ & + n_1(t) \otimes E^*_{P0}(-t) + n_1(t) \otimes n_1^*(-t)]e^{-\Gamma^* t}\} \\ & + n_2(t) \otimes \{u(t)E_{nP0}(t) \otimes E^*_{nP0}(-t)e^{-\Gamma^* t}\}. \end{aligned} \tag{3}$$

In principle, $y_P(t)$ in Eq. (2) can be deduced by subtraction between $E'_{nS}(t+T)$ and $E_{nS0}(t)$. However, the photodetector (PD) used to detect the probe light with or without the SBS gain always introduces extra noise to the subtracted signal as well as $y_P(t)$. On the basis of Eqs. (9)–(11) in [16], the signal after subtraction considering noise can be written as

$$\begin{aligned} s(t+T) &= [|E'_{nS}(t+T)|^2 + n_{\mathrm{PD1}}(t)] - [|E_{nS0}(t)|^2 + n_{\mathrm{PD2}}(t)] \\ &\approx |\Delta E_{nS}(t)|^2 + 2\,\mathrm{Re}\{\Delta E_{nS}(t)[n_2(t)]^*\} + \Delta n(t), \\ & t \geq \tau_s, \end{aligned} \tag{4}$$

where $\Delta E_{nS}(t) = E'_{nS}(t+T) - E_{nS0}(t)$ and $n_{\mathrm{PD1}}(t)$ or $n_{\mathrm{PD2}}(t)$ represent the PD noise when used to detect the probe signal with or without the SBS gain. $\Delta n(t) = n_{\mathrm{PD2}}(t) - n_{\mathrm{PD1}}(t)$ is the subtraction of these two PD noises.

Eventually, after substitution and simplification, the subtracted signal $s(t+T)$ is described by

$$s(t+T) = (g_B)^2 S(t) + (g_B)^2 N_2(t) + g_B N_3(t) + \Delta n(t), \tag{5}$$

where $(g_B)^2 S(t)$ corresponds to the term $|\frac{g_B v}{8\tau_p}\{E_{S0}(t) \otimes [u(t)y_P(t)e^{-\Gamma^* t}]\}|^2$ and is proportional to the squared ideal pulse compression of the signal to be processed $|y_P(t)|^2$, which is essentially the same as in [16]. Therefore, in Eq. (5), the term $(g_B)^2 S(t)$ is proposed as the signal of the SBS-based pulse compression and the remaining parts as the noise. $N_2(t)$ and $N_3(t)$ are given by the following:

$$\begin{aligned} N_2(t) = {} & \left(\frac{v}{8\tau_p}\right)^2 2\,\mathrm{Re}\{E_{S0}(t) \otimes [u(t)y_P(t)e^{-\Gamma^* t}]N_1^*\} \\ & + \left(\frac{v}{8\tau_p}\right)^2 |N_1(t)|^2, \end{aligned} \tag{6}$$

$$N_3(t) = \left(\frac{v}{8\tau_p}\right) 2\,\mathrm{Re}\{E_{S0}(t) \otimes [u(t)y_P(t)e^{-\Gamma^* t}]n_2^*(t)\}. \tag{7}$$

Consequently, the SNR of the SBS-based compressed result is determined by the following:

$$\mathrm{SNR} \propto \frac{\text{Signal power}}{\text{Noise power}} = \frac{\int S(t)\mathrm{d}t}{\int N_2(t) + \frac{N_3(t)}{g_B} + \frac{\Delta n(t)}{(g_B)^2}\mathrm{d}t}. \tag{8}$$

According to Eq. (8), a higher g_B gives rise to a higher SNR. To analyze the relation between SNR and g_B, a simulation of the SBS process is implemented and the result is demonstrated in Fig. 1. The signal to be processed is a 1 μs LFM pulse with a 2 GHz sweep range. The noises $n_1(t)$ and $n_2(t)$ are the environmental background noises, namely the noise floor, along with the pump and probe lightwaves before entering the fiber. The noises $n_1(t)$, $n_2(t)$, and $\Delta n(t)$ are set as white Gaussian noise in the simulation. The corresponding power spectral density (PSD) of $n_1(t)$, $n_2(t)$, and $\Delta n(t)$ is −100 dBm/Hz, −120 dBm/Hz, and −120 dBm/Hz, respectively. The PSD values are around the noise level in the experiments. The probe lightwave is a 0.2 ns pulse. The Brillouin frequency shift (BFS) is set uniformly along the fiber and $\tau_p = 10$ ns. The simulation results show the comparison of subtracted power with different g_B: 0.33 $\mathrm{m^{-1}\,W^{-1}}$, 0.60 $\mathrm{m^{-1}\,W^{-1}}$, 0.90 $\mathrm{m^{-1}\,W^{-1}}$, and 106.97 $\mathrm{m^{-1}\,W^{-1}}$, where 0.33 $\mathrm{m^{-1}\,W^{-1}}$, 0.90 $\mathrm{m^{-1}\,W^{-1}}$, and 106.97 $\mathrm{m^{-1}\,W^{-1}}$ correspond to the g_B of SMF, DCF, and an As_2Se_3 chalcogenide fiber according to [19,20], respectively. When g_B is small, only the main lobe of the compressed signal is noticeable. With the increase of g_B, the first side lobe of the signal become evident. The simulation results show that a high g_B increases the power of the signal and SNR, which matches well with the theoretical analysis. However, there is an exception when using a chalcogenide fiber with an extremely high g_B where the compressed signal is severely distorted owing to the high loss in this fiber.

To intuitively comprehend the relation between the SNR and system bandwidth, a simulation is implemented. The SNR of the compressed signal as a function of the bandwidth of the pump lightwave, under conditions of different g_B, is depicted in Fig. 2. Except for the bandwidth of the signal to be processed, other simulation parameters are set the same as in Fig. 1. According to Fig. 2, broader bandwidth of the pump light gives rise to a lower SNR. Here, we define a critical condition for the system bandwidth. Namely, the bandwidth corresponding to the SNR of 0 dB is proposed as the system bandwidth. According to the above critical condition, the system bandwidth with a g_B equal to 0.33 $\mathrm{m^{-1}\,W^{-1}}$, 0.60 $\mathrm{m^{-1}\,W^{-1}}$, 0.90 $\mathrm{m^{-1}\,W^{-1}}$, and 106.97 $\mathrm{m^{-1}\,W^{-1}}$ is 2.05 GHz, 3.60 GHz, 5.40 GHz, and 1.00 GHz, respectively.

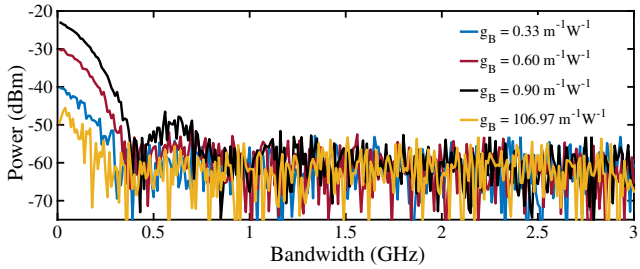

Fig. 1. Simulation results for the SBS-based pulse compression with different g_B. The pump lightwave is modulated by an LFM pulse with 2 GHz sweep range and the probe lightwave is modulated by a short pulse with 0.2 ns pulse duration. The power spectral density (PSD) of noise in the pump and probe lightwaves is set as −100 dBm/Hz and −120 dBm/Hz, respectively. The PSD from PD is −120 dBm/Hz.

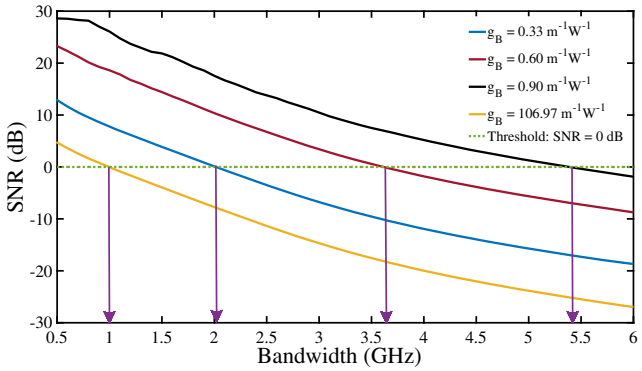

Fig. 2. Analysis of the SNR of the compressed signal as a function of the bandwidth of the pump lightwave with different g_B. The dashed line is set as the threshold of SNR = 0 dB. The pump lightwave is modulated by an LFM pulse with the sweep range from 0.5 GHz to 5 GHz and the probe lightwave is modulated by a short pulse with 0.2 ns pulse duration. The power spectral density (PSD) of noise in the pump and probe lights is set as −100 dBm/Hz and −120 dBm/Hz, respectively. The PSD from PD is −120 dBm/Hz.

It can be seen that with a higher g_B, the SNR increases; as a result, the system bandwidth is broadened. According to the analysis, wide system bandwidth requires a high SNR and, thus, a high g_B. Although a high g_B is the key parameter for the enhancement of the SNR, the corresponding broader system bandwidth, fibers with extremely high g_B, and also a high loss coefficient are not good choices for the enhancement of this SBS-based pulse compression system—for example, the As_2Se_3 chalcogenide fiber.

Thus, the optical fibers with a higher g_B (DCF) are believed to achieve the pulse compression of an ultraband microwave signal.

Figure 3 shows the experimental setup. The lightwave with a wavelength of 1550 nm is generated by the distributed-feedback laser (DFB-LD, NEL, NLK1C6DAAA) and is split into two arms by a 1 : 1 fiber coupler. In the upper arm, through an electro-optic modulator (EOM, Eospace, AX-6K5-10-PFU-PFUP-R4), the probe lightwave is modulated by a short pulse and the output is amplified by an erbium-doped fiber amplifier (EDFA1) to compensate for the power loss caused by the modulator. The short pulse is generated via a pulse generator (Tektronix, PSPL10070A). In the lower arm, a single sideband

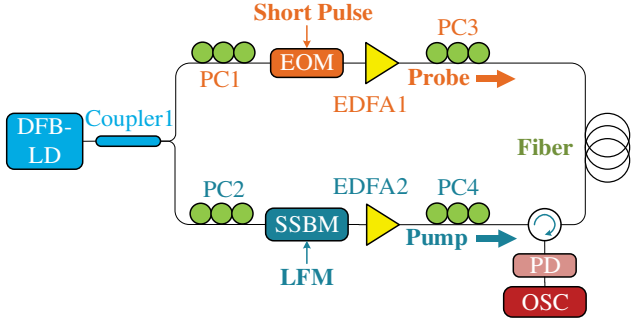

Fig. 3. Experimental setup for pulse compression of the broadband microwave frequency based on the SBS process. DFB-LD, distributed-feedback laser; PC, polarization controller; EOM, electro-optic modulator; EDFA, erbium-doped fiber amplifier; SSBM, single sideband modulator; PD, photo-detector; and OSC, oscilloscope.

modulator (SSBM) is used to modulate the signal to be processed. The first higher sideband (in frequency) of the modulated signal is selected after the SSBM. The output of the SSBM is amplified by EDFA2. Polarization controllers (PC1, PC2) optimize the light polarizations before the modulators. PC3 and PC4 are used to ensure the maximum SBS interaction in an optical fiber. After PC3 and PC4, the probe light and the pump light counter-propagate along the optical fiber and interact with each other. To isolate the pump light and transmit the amplified probe light, a circulator is used after PC4. A PD converts the detected probe power into the electric signal, namely, the compressed signal, which is observed through the oscilloscope (OSC, Tektronix, DSA70804). To reduce noise and distortion in the pulse compression system as much as possible, this setup is simplified by using two modulators rather than three modulators as in [16]. The beat frequency between the pump and probe lightwaves is the start frequency of the pump lightwave, which should be the BFS of the optical fibers.

Experiments using two different fibers (SMF and DCF) under the same conditions are implemented and compared. The BFS of the SMF and the DCF is 10.812 GHz and 9.672 GHz, respectively. The g_B of the SMF and the DCF is ∼0.3 m^{-1} W^{-1} and ∼0.9 m^{-1} W^{-1}, respectively. The pump lightwave is modulated by an LFM pulse signal to be processed, which is generated via an arbitrary waveform generator (AWG, Keysight, M8195A). The duration of the LFM pulse is set as 3.6 μs and the frequency is linearly swept from the BFS of the fiber with different sweep ranges. The power of the pump and probe lightwaves before entering fibers is around 22.29 dBm and 10.67 dBm, respectively. Each experimental result using DCF is acquired after averaging by the OSC 30 times instead of 1000 times in [16].

Figure 4 depicts the pulse compression results using the SMF and DCF compared with the squared ideal pulse compressions of the LFM signal under two bandwidths of 200 MHz and 1 GHz. The short pulse duration is set as 500 ps. It can be seen that the compressed results with the

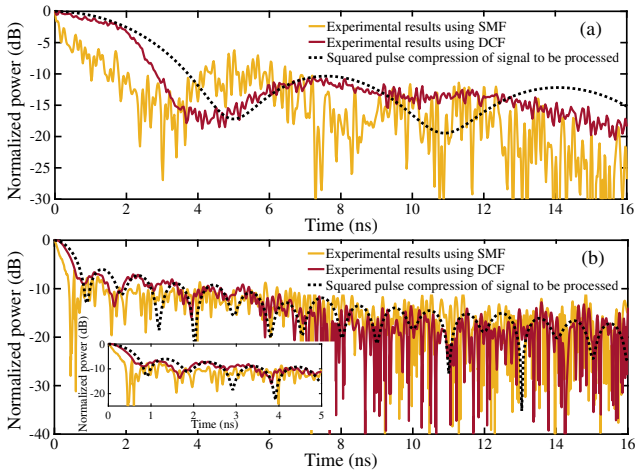

Fig. 4. Experimental results for the pulse compression based on the SBS process with different bandwidth of the LFM signal. The pulse compression results with both SMF and DCF are compared with the squared ideal pulse compressions of the LFM pulses. The duration of the short probe pulse is 500 ps and the sweep ranges of the LFM pulses are (a) 200 MHz and (b) 1 GHz, respectively.

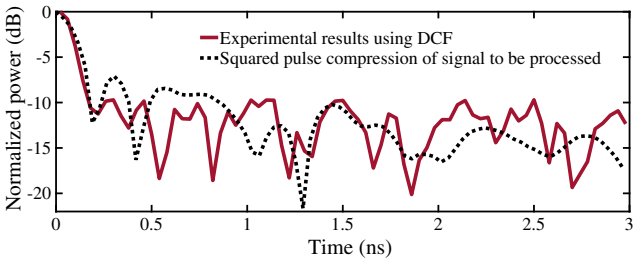

Fig. 5. Experimental results for the pulse compression based on the SBS process. The pulse compression results achieved by the subtraction are compared with the squared ideal pulse compressions of the LFM pulses with 5 GHz bandwidth.

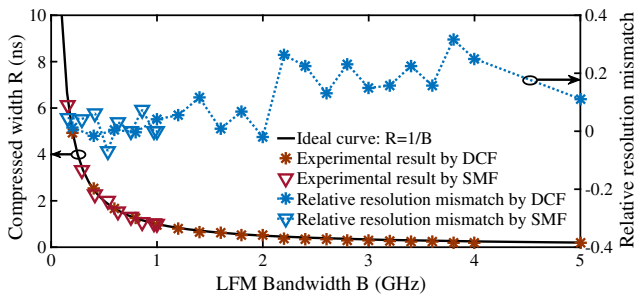

Fig. 6. Full width of the compressed main lobe as a function of the sweeping bandwidth of the LFM pulse. The mismatch between the compressed width and the ideal width is depicted by the dashed curve.

SMF and DCF maintain the same shape of pulse compression and the main lobe of the SMF and DCF is evident. However, thanks to the greater g_B and, consequently, larger signal power, as well as the SNR, the identification of the peak of the main lobe of the compressed signal is more precise. Thus, the compressed result with the DCF matches better with the ideal pulse compression than the SMF. According to [16], the range resolution R for the compressed signal is defined as the width between the peak and the first null, which approximately equals the reciprocal of the bandwidth B of the LFM pulse. Comparing Figs. 4(a) and 4(b) with the increase of B, R of the compressed signal is shortened. Furthermore, owing to the high g_B, the system bandwidth by using the DCF can easily reach 1 GHz, whereas the compressed signal by using the SMF is severely affected by noise and the larger system bandwidth can no longer be reached by using the SMF.

To guarantee the capability of the pulse compression of an ultrabroad bandwidth (such as 5 GHz), the probe pulse duration is set as 200 ps. Figure 5 depicts the pulse compression result of an LFM signal with 5 GHz bandwidth by using the DCF. The main lobe of the compressed result fits well with the ideal curve. The mismatch between the experimental result and the ideal curve is caused by the insufficient Brillouin gain for the ultrashort probe pulse.

The range resolution R of the LFM pulses with the different bandwidth B by using the DCF compared with the $R-B$ data, by using the SMF in [16], is compared in Fig. 6. It shows a clear inverse relation between the R and B of the LFM pulse for both the SMF and DCF. The approachable system bandwidth with the DCF is significantly larger than that with the SMF. Moreover, the relative error of R between the experimental result and the ideal $R-B$ curve is smaller by using the DCF. The comparison between the SMF and DCF indicates that, by increasing the g_B, the performance of the SBS-based pulse compression is enhanced.

To conclude, we have analyzed and enhanced the SNR of the SBS-based pulse compression of a broadband microwave system. Based on the analysis, a higher g_B gives rise to a higher SNR and, thus, a broader system bandwidth. Experiments are carried out by using the DCF and SMF to verify the analysis. The SNR of the compressed signal is enhanced and the detected signal also matches well with the ideal pulse compression signal by using the DCF with the higher g_B. Consequently, the system bandwidth can be extended to 5 GHz.

Funding. National Natural Science Foundation of China (NSFC) (61535006, 61571292).

REFERENCES

1. E. C. Farnett and G. H. Stevens, *Radar Handbook* (McGraw-Hill, 1990).
2. D. K. Barton, *Modern Radar System Analysis* (Artech House, 1988), p. 607.
3. D. Morgan, Ultrasonics **11**, 121 (1973).
4. R. Milleit, IEEE Trans. Aerosp. Electron. Syst. **AES-6**, 73 (1970).
5. E. Mosca, IEEE Trans. Inf. Theory **13**, 131 (1967).
6. P. Ghelfi, F. Laghezza, F. Scotti, G. Serafino, A. Capria, S. Pinna, D. Onori, C. Porzi, M. Scaffardi, A. Malacarne, V. Vercesi, E. Lazzeri, F. Berizzi, and A. Bogoni, Nature **507**, 341 (2014).
7. W. Zou, H. Zhang, X. Long, S. Zhang, Y. Cui, and J. Chen, Sci. Rep. **6**, 19786 (2016).
8. G. C. Valley, Opt. Express **15**, 1955 (2007).
9. A. Khilo, S. J. Spector, M. E. Grein, A. H. Nejadmalayeri, C. W. Holzwarth, M. Y. Sander, M. S. Dahlem, M. Y. Peng, M. W. Geis, N. A. DiLello, J. U. Yoon, A. Motamedi, J. S. Orcutt, J. P. Wang, C. M. Sorace-Agaskar, M. A. Popoviä, J. Sun, G. Zhou, H. Byun, J. Chen, J. L. Hoyt, H. I. Smith, R. J. Ram, M. Perrott, T. M. Lyszczarz, E. P. Ippen, and F. X. Kärtner, Opt. Express **20**, 4454 (2012).
10. G. Yang, W. Zou, L. Yu, K. Wu, and J. Chen, Opt. Express **24**, 24061 (2016).
11. J. Capmany and D. Novak, Nat. Photonics **1**, 319 (2007).
12. J. Zhang and J. Yao, Optica **1**, 64 (2014).
13. H. Zhang, W. Zou, and J. Chen, Opt. Lett. **40**, 1085 (2015).
14. W. Zou, S. Yang, X. Long, and J. Chen, Opt. Express **23**, 512 (2015).
15. D. Marpaung, B. Morrison, M. Pagani, R. Pant, D. Choi, B. Luther-Davies, S. J. Madden, and B. J. Eggleton, Optica **2**, 76 (2015).
16. X. Long, W. Zou, and J. Chen, Opt. Express **24**, 5162 (2016).
17. X. Long, W. Zou, and J. Chen, Opt. Express **25**, 2206 (2017).
18. G. P. Agrawal, *Nonlinear Fiber Optics* (Academic, 2007).
19. A. Kobyakov, M. Mehendale, M. Vasilyev, S. Tsuda, and A. Evans, J. Lightwave Technol. **20**, 1635 (2002).
20. J. Sanghera, C. Florea, L. Shaw, P. Pureza, V. Nguyen, M. Bashkansky, Z. Dutton, and I. Aggarwal, J. Non-Cryst. Solids **354**, 462 (2008).